Proceedings of the Seventh International Conference on
Railway Technology: Research, Development and Maintenance
Edited by: J. Pombo
Civil-Comp Conferences, Volume 15, Paper 12.5
Civil-Comp Press, Edinburgh, United Kingdom, 2026
ISSN: 2753-3239, doi: 10.4203/ccc.15.12.5

Three-Dimensional Finite Element Analysis of Cyclic Deformation of Ballast Beds at Rail Joints Using Grid-Type Sleepers

K. Koro[1] and H. Kanai[2]

[1] Department of Civil Engineering, Niigata University, Japan
[2] Master's Program, Graduate School of Integrated Arts and Sciences, Niigata University, Japan

Abstract

This study investigates the influence of the geometric dimensions and material parameters of grid-type sleepers on the cyclic deformation of ballast beds in jointed railway tracks. A sensitivity analysis is performed using a three-dimensional finite element (FE) method with an elastoplastic constitutive model based on the cyclic densification model. The results indicate that an imbalance in the maximum railpad force around the rail joint induces residual rigid-body rotation of the grid-type sleeper, which becomes more pronounced with decreasing longitudinal bending stiffness. In addition, reducing the sleeper density increases ballast settlement due to enhanced residual deformation in the low-cycle regime, although this effect diminishes with increasing number of loading cycles.

Keywords: ballast settlement, grid-type sleeper, elastoplastic FEM, cyclic densification model, wheel-track vibration

1 Introduction

The grid-type sleeper [1] is a concrete sleeper characterized by a structural configuration in which several conventional transverse sleepers are arranged directly beneath the rails and integrally connected by longitudinal sleeper members. Wada et al. [1] demonstrated, through field observations, its effectiveness in mitigating track deterioration at rail joints. The authors [2] proposed a finite element (FE)-based simulation method for wheel-track vibration analysis of jointed railway tracks incorporating grid-type sleepers. Furthermore, a coupled simulation method has been developed to evaluate the vibration response of grid-type sleepers and the cyclic deformation behavior of the ballast bed for design and construction applications [3]. However, previous studies have focused on straight track sections and have investigated the cyclic deformation characteristics within the longitudinal track profile at locations directly beneath the rail using two-dimensional simulations. Three-dimensional numerical simulations of ballast beds beneath grid-type sleepers at rail joints have not yet been conducted.

In this paper, a three-dimensional cyclic elastoplastic finite element analysis of the ballast bed is performed, focusing on rail joints equipped with grid-type sleepers. The analysis employs a cyclic densification model proposed by Suiker et al. [4]. Through a series of numerical analyses with varying geometric dimensions and material parameters of the grid-type sleepers, the effectiveness of grid-type sleepers in suppressing the deterioration of ballasted tracks around rail joints is investigated.

2 Modeling of vibration phenomena in jointed track with grid-type sleepers

In the present paper, wheel-track vibration analysis is employed to evaluate the maximum railpad force (i.e., the maximum rail-sleeper interaction force) in a ballasted track with a rail joint and a grid-type sleeper. Figure 1 depicts the wheel-track vibration model of the track. The model consists of masses, dashpots, contact springs, beams, and a Winkler elastic foundation [5].

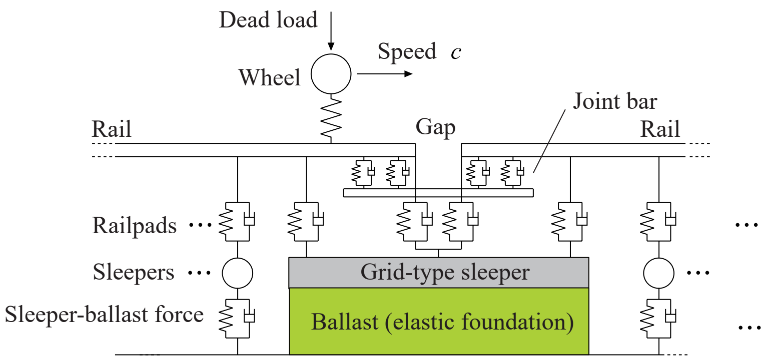

Figure 1: Wheel-track vibration model

The rail and joint bars are modeled as Bernoulli-Euler's beams with uniform cross-sections. The governing equations of rail, discretized by the FEM, is expressed as

$$[\boldsymbol{M}_r]\{\ddot{\boldsymbol{U}}_r(t)\}+[\boldsymbol{K}_r]\{\boldsymbol{U}_r(t)\} = [\boldsymbol{G}_c(t)]\{\boldsymbol{P}(t)\}-[\boldsymbol{G}_{rp}]\{\boldsymbol{F}_{rp}(t)\}-[\boldsymbol{G}_{jb}]\{\boldsymbol{F}_{jb}(t)\}, \quad (1)$$

where $(\dot{\ }) = \partial/\partial t$ (t: time), and $\{\boldsymbol{U}_r\}$ is the nodal vector on the rail displacement. $[\boldsymbol{K}_r]$ and $[\boldsymbol{M}_r]$ are the stiffness- and the mass matrices. ρ is the density, A is the cross sectional area and EI is the bending stiffness. $\{\boldsymbol{F}_{jb}\}$ is the conecting force vectors on the joint bar and the rail. $\{\boldsymbol{F}_{rp}\}$ is the nodal force of railpads. $\{\boldsymbol{P}\}$ is the wheel-rail contact force. $[\boldsymbol{G}_{jb}]$, $[\boldsymbol{G}_{rp}]$ and $[\boldsymbol{G}_c]$ are the matrices for transforming $\{\boldsymbol{F}_{jb}\}$, $\{\boldsymbol{F}_{rp}\}$ and $\{\boldsymbol{P}\}$ to those nodal value vectors.

The grid-type sleeper is represented as a beam with a variable cross-section supported by an elastic foundation. The weak form of the grid-type sleeper is expressed as follows:

$$[\boldsymbol{M}_{gs}]\{\ddot{\boldsymbol{U}}_{gs}(t)\} + [\boldsymbol{K}_{gs}]\{\boldsymbol{U}_{gs}(t)\} = [\boldsymbol{G}_{grp}]\{\boldsymbol{F}_{rp}(t)\} - [\boldsymbol{G}_{ef}]\{\boldsymbol{F}_b(t)\} \quad (2)$$

where $\{\boldsymbol{U}_{gs}\}$ is the nodal displacement vector of the grid-type sleeper. $[\boldsymbol{K}_{gs}]$ and $[\boldsymbol{M}_{gs}]$ are the stiffness- and the mass matrices. $[\boldsymbol{G}_{grp}]$ is the matrix for transforming the railpad force $\{\boldsymbol{F}_{rp}\}$ to the nodal value vector. The sleeper reaction $F_{b,i}(i = 1, 2, \cdots, n_e)$ is governed by $F_{b,i} = k_{b,i}(u_{gs,i} - u_{b,i})$.

The railpad force is modeled as a Voigt unit as

$$F_{rp,j} = k_{rp,j}(u_{rp,j} - u_{slp,j}) + \eta_{rp,j}(\dot{u}_{rp,j} - \dot{u}_{slp,j}) \quad (3)$$

where $u_{slp,j}$ is the vertical displacement of sleeper. $k_{rp,j}$ and $\eta_{rp,j}$ are the spring constants and the damping coefficients of the jth railpad. The maximum of each railpad force are used as the external force in the cyclic deformation analysis of ballast beds.

Conventional sleepers are modeled as lumped masses. The equations of motion on the lumpted masses are given by

$$m_{slp,j}\ddot{u}_{slp,j} = F_{rp,j} - \tilde{F}_{sb,j} + m_{slp,j}g \quad (4)$$

where $m_{slp,j}$ is the mass of the jth sleeper, and the sleeper reaction $\tilde{F}_{sb,j}$ is defined as

$$\tilde{F}_{sb,j} = k_{sb,j}\langle u_{slp,j} - u_{blst,j}\rangle \quad (5)$$

where $k_{sb,j}$ is the spring constant at the jth sleeper, and $u_{blst,j}$ is the ballast displacement. $\langle \cdot \rangle$ is Macauley bracket.

The two wheels are modeled as moving masses traveling at a constant speed c. The equations of motion of the two wheels are given by

$$m_{wh,i}\ddot{u}_{wh,i} = P_b - P_i + m_{wh,i}g \quad (6)$$

where $i = 1, 2, \ldots, N_{wh}$ and P_b is the dead load. $m_{wh,i}$ is the mass of the ith wheel and P_i is the contact force between the ith wheel and the rail. $u_{wh,i}$ is the vertical displacement of the ith wheel. g is the gravity.

The wheel-rail contact force P_i ($i = 1, 2, \ldots, N_{wh}$), which is the component of the vector $\{\boldsymbol{P}\}$, is evaluated based on Hertzian contact theory. The force is influenced by the contact state around a rail joint, and thus is defined as

$$P_i = \kappa_i k_{cnt,i}(u_{wh,i} - u_{c,i} - S(x_{c,i}))^{\frac{3}{2}} \tag{7}$$

where $u_{c,i}$ is the rail deflection at the contact point of the wheel, and $S(x_{c,i})$ is the rail surface profile. $k_{cnt,i}$ is the contact spring coefficient which depends on Young's modulus, Poisson's ratios of the wheels and the rails and the curvature of the contact surface. κ_i ($0 < \kappa \leq 1, i = 1, 2, \ldots, N_{wh}$) is the reduction factor of the contact spring coefficients $k_{cnt.i}$ [5].

3 Elastoplastic modeling of cyclic deformation of ballast beds

In the present study, the elastoplastic response of ballast beds is evaluated using a three-dimensional finite element method (3D FEM) with a cyclic densification model [4]. This constitutive model consists of a monotonic loading model and a cyclic loading model. In the 3D FE analysis, the external loads are given by the maximum force at each railpad, obtained from the wheel-track vibration analysis.

3.1 Motonic loading model

The monotonic loading model is employed in the monotonic loading / unloading process. The constitutive equations is expressed as

$$\dot{\sigma}_{ij} = D_{ijkl}(p)\Big(\dot{\varepsilon}_{kl} - \dot{\varepsilon}^p_{kl}\Big), \tag{8}$$

$$D_{ijkl}(p) = \frac{3K_{ref}}{2(1+\nu)}\left(\frac{p}{p_{ref}}\right)^{1-n^e}\Big[(1-2\nu)(\delta_{ik}\delta_{jl} + \delta_{il}\delta_{jk}) + 2\nu\delta_{ij}\delta_{kl}\Big], \tag{9}$$

where σ_{ij} is the stress tensor, ε_{kl} is the strain tensor, and ε^p_{kl} is the plastic strain tensor. $p = \sigma_{kk}/3$, and ν is Poisson's ratio, K_{ref}, n^e and p_{ref} are the material parameters which controls elastic response of the ballast beds.

Plastic deformation is assumed to occur under three failure mechanisms: frictional sliding, volumetric compression, and tensile failure. The yield functions corresponding to these three failure modes, f^f, f^c, and f^t, are defined as follows:

$$\begin{aligned} f^f(q, p, \kappa^p_0) &= -\frac{q}{p - p^t_{num}} - H^f(\kappa^p_0) = 0, \\ f^c(p, \varepsilon_{vol,c,0}) &= \frac{p}{P_0} - H^c(\varepsilon_{vol,c,0}) = 0, \\ f^t(p) &= p - p^t = 0, \end{aligned} \tag{10}$$

where $q = \sqrt{3s_{ij}s_{ij}/2}$ and $s_{ij} = \sigma_{ij} - p\delta_{ij}$.

The hardening functions H^f and H^c in Eq.(4) are defined as

$$\begin{aligned} &H^f(\kappa_0^p) = H_0 + (H_m - H_0)\big[1 - \exp(-\zeta^f \kappa_0^p)\big], \\ &H^c(\varepsilon_{vol,c,0}) = 1 + \zeta^c \varepsilon_{vol,c,0}^p \end{aligned} \tag{11}$$

where κ_0^p and $\varepsilon_{vol,c,0}^p$ are the plastic multipliers associated with frictional sliding and volumetric compression. P_0, H_0, H_m, ζ^f and ζ^c are material parameters.

The plastic flow rule in this model is formulated using a non-associated rule, as follows:

$$\dot{\varepsilon}_{ij}^p = \dot{\kappa}_0^p \frac{\partial G^f(q, p, \kappa_0^p)}{\partial \sigma_{ij}} + \dot{\varepsilon}_{vol,c,0}^p \frac{\partial G^c(p, \varepsilon_{vol,c,0}^p)}{\partial \sigma_{ij}} + \dot{\varepsilon}_{vol,t,0}^p \frac{\partial G^t(p)}{\partial \sigma_{ij}} \tag{12}$$

where $\dot{\varepsilon}_{vol,t,0}^p$ is the strain rate associated with the tensile failure. The plastic potential functions G^f, G^c and G^t are defined as

$$\begin{aligned} &G^f(p, q, \kappa_0^p) = q + D^f(\kappa_0^p)p, \quad D^f(\kappa_0^p) = D_0 + (D_m - D_0)\big[1 - \exp(-\zeta^f \kappa_0^p)\big], \\ &G^c(p, \varepsilon_{vol,c,0}^p) = -p + H^c(\varepsilon_{vol,c,0}^p)P_0, \quad G^t(p) = f^t(p), \end{aligned} \tag{13}$$

where D_0 and D_m are the material parameters.

3.2 Cyclic loading model

The cyclic loading constitutive model is used to describe the accumulation of permanent deformation under cyclic loading with a constant amplitude. The constitutive equations are defined as follows:

$$\frac{\mathrm{d}\sigma_{ij}}{\mathrm{d}N} = D_{ijkl}(p) \left(\frac{\mathrm{d}\varepsilon_{kl}}{\mathrm{d}N} - \frac{\mathrm{d}\varepsilon_{kl}^p}{\mathrm{d}N} \right) \tag{14}$$

where N is the number of loading/unloading cycles.

The plastic strain ε_{ij}^p is described by the following equations based on a non-associated flow rule, considering the three failure mechanisms: frictional sliding, volumetric compression, and tensile failure.

$$\frac{\mathrm{d}\varepsilon_{ij}^p}{\mathrm{d}N} = \frac{\mathrm{d}\kappa^p}{\mathrm{d}N} \frac{\partial g^f(q, p, \kappa^p)}{\partial \sigma_{ij}} + \frac{\mathrm{d}\varepsilon_{vol,c}^p}{\mathrm{d}N} \frac{\partial g^c(p, \varepsilon_{vol,c}^p)}{\partial \sigma_{ij}} + \frac{\mathrm{d}\varepsilon_{vol,t}^p}{\mathrm{d}N} \frac{\partial g^t(p)}{\partial \sigma_{ij}} \tag{15}$$

where the plastic potential g^f, g^c and g^t are given by

$$\begin{aligned} &g^f(p, q, \kappa^p) = q + d^f(\kappa^p)p, \quad d^f(\kappa^p) = d_0 + (d_m - d_0)\big[1 - \exp(-\zeta^f \kappa^p)\big], \\ &g^c(p, \varepsilon_{vol,c}^p) = -p + h^c(\varepsilon_{vol,c}^p)p_0, \;\; g^t(p) = f^t(p), \end{aligned} \tag{16}$$

where p_0, d_0 and d_m is the material parameters.

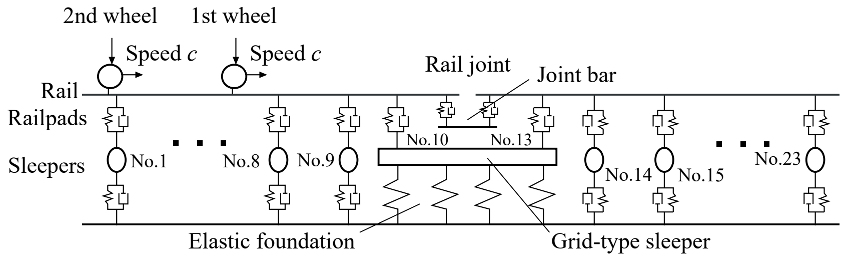

Figure 2: Test jointed track.

In Eq.(15), The plastic multipliers κ^p and $\varepsilon^p_{vol,c}$ are evaluated by integrating the following equations on the number of cycles N:

$$\begin{aligned} \frac{\mathrm{d}\kappa^p}{\mathrm{d}N} &= \alpha^f \left\langle -\frac{q}{p - p^t_{num}} - h^f_{sh}(\kappa^p) \right\rangle^{\gamma^f}, \\ \frac{\mathrm{d}\varepsilon^p_{vol,c}}{\mathrm{d}N} &= \alpha^c \left\langle \frac{p}{p_0} - h^c_{sh}(\varepsilon^p_{vol,c}) \right\rangle^{\gamma^c} \end{aligned} \tag{17}$$

where α^f, α^c, γ^f and γ^c are the material parameters.

The shakedown stresses h^f_{sh} and h^c_{sh}, which are the threshold for the onset of plastic strain rate in the cyclic loading model, are formulated with the parameters η^f, η^c, h_0. h_m as

$$\begin{aligned} h^f_{sh}(\kappa^p) &= h_0 + (h_m - h_0)\big[1 - \exp\{-\eta^f \cdot (\kappa^p - \kappa^p_0)\}\big], \\ h^c_{sh}(\varepsilon^p_{vol,c}) &= 1 + \eta^c(\varepsilon^p_{vol,c} - \varepsilon^p_{vol,c,0}) \end{aligned} \tag{18}$$

4 Influence of geometric dimensions and material parameters of a grid-type sleeper on ballast settlement

We investigate the influence of the geometric dimensions and material parameters of a grid-type sleeper on the cyclic deformation of ballast beds.

The wheel-track vibration analysis is conducted for a jointed track consisting of two rails supported by eighteen sleepers and a grid-type sleeper (see Figure 2). The grid-type sleeper is arranged on the ballast bed beneath the rail joint. The ballast beds is modeled as elastic foundation. The time increment is 1.0×10^{-3}(s). Two wheels with a spacing of 2.1 (m) and a dead load of 50(kN) travel along the track under the running speed 30m/s. The rails used JIS 50N rails without surface profile. The rail joint is arranged at the central point of $x = 5.7$(m), and has the 5mm gap. Table 1 shows the parameter setting of the track.

The geometric dimensions and the material parameters of a grid-type sleeper is indicated in Table 2.

In the ballast cyclic deformation analysis, a 3D FEM is used to evaluate the cyclic deformation behavior of the jointed track with a grid-type sleeper and four conventional sleepers, as shown in Figure 3. The sleepers are modeled as elastic media. The

Table 1: Prescribed parameters for vibration analysis.

Rail	
Young's modulus (GPa)	206
Poisson's ratio	0.3
Density (kg/m^3)	7850
Area (m^2)	64.29×10^{-4}
Moment of inertia (m^4)	1960×10^{-8}
Radius of curvature R(m)	0.3
Sleeper	
mass (kg)	80
Width (m)	0.24
Spacing (m)	0.36
Wheels	
Young's modulus (GPa)	206
Poisson's ratio	0.3
Mass (kg)	697
Radius (m)	0.43

Joint bar	
Young's modulus (GPa)	206
Density (kg/m^3)	7850
Area (m^2)	67.72×10^{-4}
Moment of inertia	606×10^{-8}
Railpads	
Spring const. (MN/m)	110
Damping Coef. (kNsec/m)	98
Sleeper-ballast	
Spring const. (MN/m)	74
Damping Coef. (kNsec/m)	49
Ballast beds	
Young's modulus (MPa)	88
Poisson's ratio	0.28
Density (kg/m^3)	1.7×10^3

Table 2: Prescribed parameters of a grid-type sleeper.

Young's modulus(GPa)	33
Density(kg/m^3)	2.5×10^3
Poisson's ratio	0.17
longitudinal members	
Area (m^2)	7.0×10^{-2}
Moment of inertia (m^4)	1786×10^{-7}
joint region	
Area (m^2)	13.1×10^{-2}
Moment of inertia(m^4)	3350×10^{-7}

constitutive models of the ballast bed is given by the cyclic densification model. We fixed the number of cycles N at 500.

4.1 Influence of geometric dimensions

We now investigate the influence of the geometric dimensions of a grid-type sleeper on the cyclic deformation behavior of ballast beds. The design variables of the grid-type sleeper are the widths b_1 and b_2, the height h and the length l. The setting value of the design variables are shown in Table 3. "Case 0" indicates the results which are obtained under the default settings of the geometric dimensions. In each case, the geometric dimensions except for the design variables is given by the values indicated in Table 2.

Figure 4 illustrates the time history of the railpad force. The maximum railpad force at each railpad (Nos. 8-15) occurs immediately before the passage of the second wheel. Its magnitude increases at No.13, which is one of the two railpads closest to the rail joint, due to the wheel load impact induced by the joint passage. The imbalance between this force and that at No. 10, the other railpad located on the

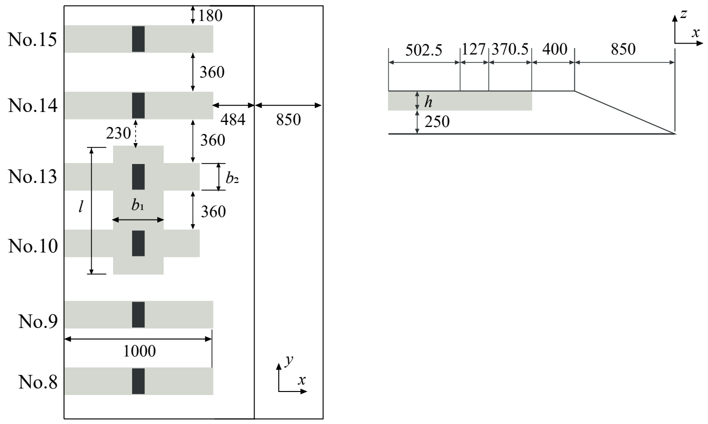

Figure 3: Ballast beds and sleepers

Table 3: Design variables for geometric dimensions of a grid-type sleeper.

case	variables	setting values
Case 1	Width b_1(m)	0.30
Case 2	Width b_1(m)	0.50
Case 3	Width b_2(m)	0.30
Case 4	Height h(m)	0.25
Case 5	Height h(m)	0.13
Case 6	Length l(m)	1.16

grid-type sleeper. The deformation of the ballast bed caused by repeated loading is thus expected to become larger in front of the rail joint, leading to the rotation of the grid-type sleeper.

Table 4 shows the variation rate of the maximum railpad force at No.13 for each test case. The maximum force at No.13 depends on the setting of the height of the grid-type sleepers. In Case 4, where the sleeper height is increased by 50%, the maximum force decreases by approximately 3%, whereas in Case 5, where the sleeper height is reduced by 25%, the maximum force increases by 1.35%. These results suggest that increasing the stiffness of the grid-type sleeper is effective in reducing the external forces acting on the track.

Figure 5 shows the ballast settlement in longitudinal direction beneath the rail. At a rail joint equipped with a grid-type sleeper, the sleeper height is identified as the most sensitive parameter affecting ballast settlement. In Case 5, where the sleeper height is reduced, the decrease in the longitudinal bending stiffness of the grid-type sleeper results in a slight influence of bending deformation on the settlement profile. The reduction in sleeper stiffness leads to a more pronounced rigid-body rotation of the grid-type sleeper. Moreover, the results of Case 6 indicate that increasing the length of the longitudinal sleeper causes bending deflection at its ends, which affects the settlement profile.

Figure 6 depicts the root of the second invariant on the permanent deviator strain for Case 0, 2, 5 and 6. The second invariant of the deviatoric strain, which indicates the

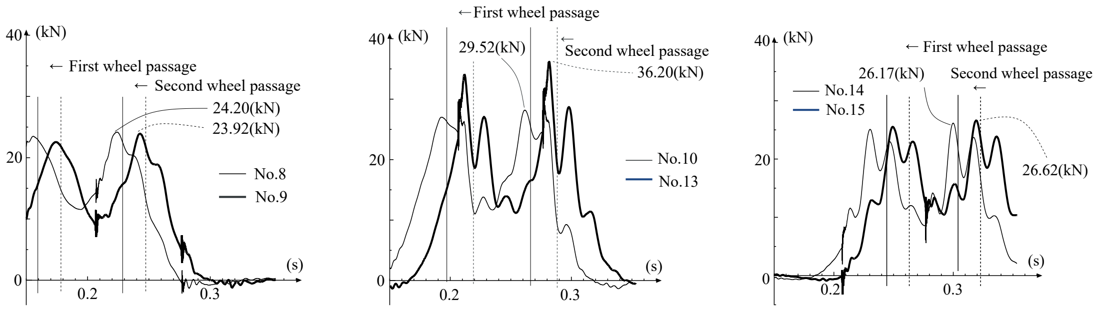

(i)Railpads No.8 and 9 (ii)Railpads No.10 and 13 (iii)Railpads No.14 and 15

Figure 4: Time histories of the railpad force in Case 0.

Table 4: Variation rate of the maximum railpad force at No.13 for each test case.

Case	F_{max} (kN)	Variation rate[%]
Case 0	36.20	0.00
Case 1	35.80	-1.10
Case 2	36.38	+0.50
Case 3	36.19	-0.03
Case 4	35.14	-2.93
Case 5	36.69	+1.35
Case 6	36.19	-0.03

locations of concentrated shear deformation, becomes large around the perimeter and corners of the sleeper, as well as beneath the sleeper. This is because the stiffness of the sleeper is higher than that of the ballast, causing the ballast to deform in a manner close to rigid indentation.

4.2 Influence of material parameters

In this subsection, we investigate the influence of the material parameters of the grid type sleeper on the cyclic deformation behavior of the ballast beds. The design variables of are Young's modulus and the density. The setting value of the design variables are shown in Table 5. "Case 0" indicates the results which are obtained under the default settings of the geometric dimensions. In each case, the material parameters except for the design variables is given by the values indicated in Table 2.

Table 6 shows the variation rate of the maximum railpad force at No.13 for each test case. The influence of variations in material parameters on the maximum railpad force at No.13 is relatively small compared with that of changes in geometric dimensions.

Figure 7 shows the ballast settlement in longitudinal direction beneath the rail. As shown in Table 6, although the maximum railpad force is smaller when the density of the sleeper is reduced, the settlement displacement becomes larger than that in Case 0. This is attributed to the reduced sleeper weight acting on the ballast bed at the onset of loading, which results in cyclic loading being applied from an insufficiently com-

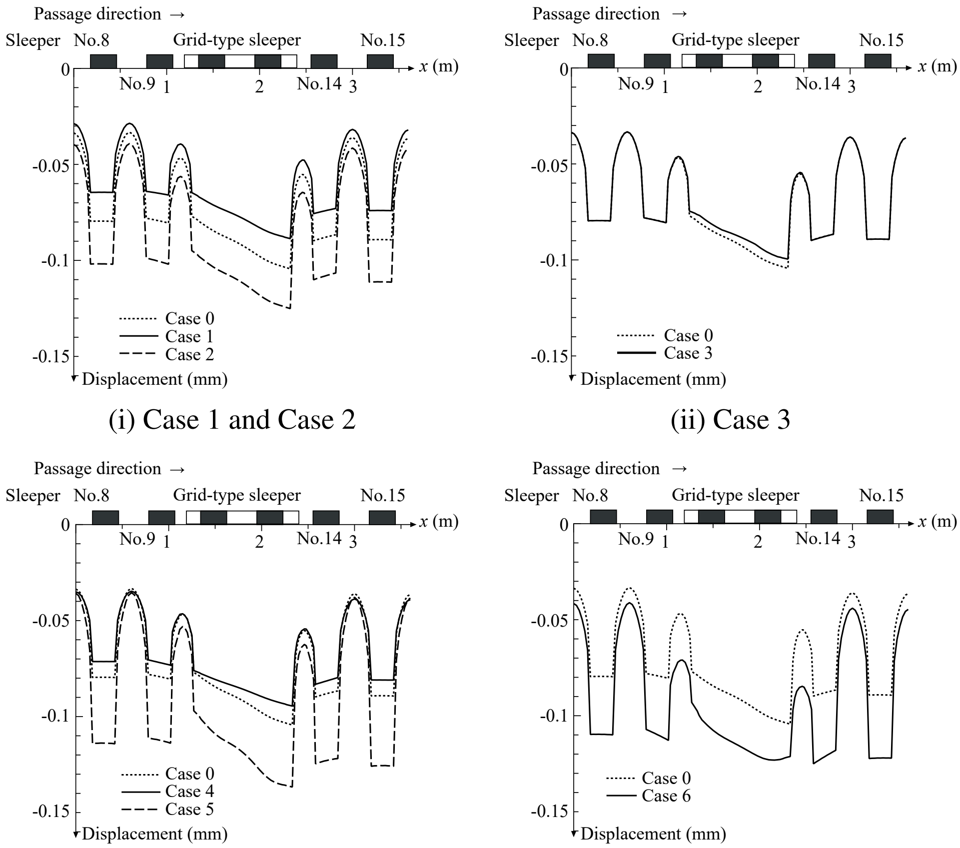

(i) Case 1 and Case 2

(ii) Case 3

(iii) Case 4 and Case 5

(iv) Case 6

Figure 5: Ballast settlement in longitudinal direction for Case 0 – 6.

pressed state of the ballast, thereby promoting significant development of settlement displacement in the early stage of loading. Hence, the influence of the sleeper density on ballast settlement is expected to become relatively smaller as the number of loading cycles N increases and settlement accumulates.

5 Conclusion

In the present study, we investigated the influence of the geometric dimensions and the material parameters of a grid-type sleeper on the cyclic deformation of ballast beds in a jointed railway track. The design variables of the grid-type sleeper include the width, height, and length of the longitudinal members, as well as Young's modulus and density. A sensitivity analysis of these design variables is conducted using a three-dimensional finite element (FE) method with an elastoplastic model. The constitutive behavior of the ballast bed is described by a cyclic densification model proposed by Suiker et al. [4].

In the track vibration response, an imbalance in the maximum railpad force occurs before and after the rail joint. As a result, residual rigid-body rotation of the grid-type

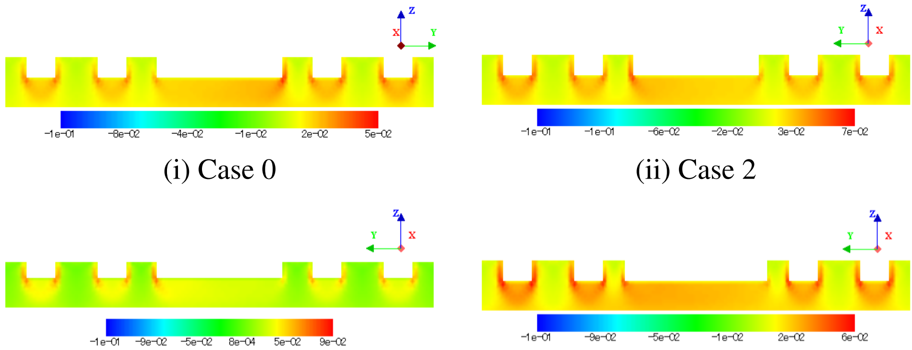

(i) Case 0 (ii) Case 2

(iii) Case 5 (iv) Case 6

Figure 6: Distribution of the root of the second invariant of the permanent deviator strain for Case0, 2, 5 and 6 (%).

Table 5: Design variables for material parameters of a grid-type sleeper.

case	variables	setteing values
7	Young's modulus(GPa)	40
8	Young's modulus(GPa)	30
9	Density(kg/m^3)	2.60×10^3
10	Density(kg/m^3)	2.30×10^3

sleeper is observed under all design conditions. In particular, a reduction in the longitudinal bending stiffness of the sleeper leads to more pronounced rigid-body rotation. Furthermore, the numerical simulations show that reducing the density of the grid-type sleeper leads to an increase in ballast settlement. This is attributed to the reduced weight of the sleeper, which promotes the development of residual deformation in the low-cycle regime. Hence, the influence of mass density is expected to decrease as the number of loading cycles increases.

Accknowledgement
This work was supported by JSPS KAKENHI Grant Number JP25K07899.

References

[1] Wada, T., Seya, M and Harada, A.: Development of a Multiple Tie Tamper-compatible Grid Type Sleeper that Reduces Lateral Force at Rail Joints. *JR EAST Tech. Rev.*, No.22-Spr. 2012, pp.59-62, 2012.

[2] Koro, K., Kono, A. and Abe, K.: FE-based simulation method on wheel-track vibration of jointed railway track with grid-type sleepers. *Jounal of JSCE A2(Applied Mechanics)*, Vol.77, No.2, pp.I_239-I_249, 2022 (in Japanese).

[3] Koro, K.: Influence of material parameters and shape dimensions of grid-type sleeper on settlement and vibration of ballasted railway track. *Journal of Railway Engineering JSCE*, Vol.29, No.1, pp.240-247, 2025 (in Japanese).

Table 6: Variation rate of the maximum railpad force at No.13 for each test case.

Case	$F_{\max}$ (kN)	Variation rate[%]
Case 7	36.18	-0.06
Case 8	36.22	+0.06
Case 9	36.33	-0.14
Case 10	36.33	-0.14

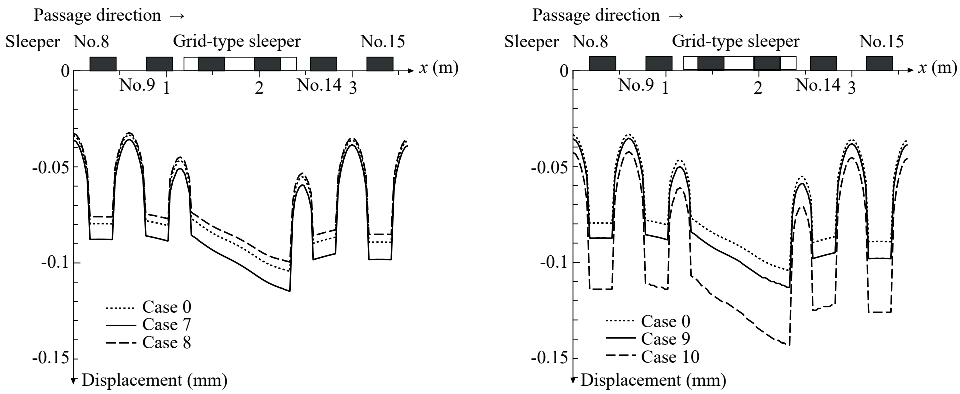

(i) Case 7 and Case 8 (ii) Case 9 and Case 10

Figure 7: Ballast settlement in longitudinal direction for Case 7 – 10.

[4] Suiker, A.S.J., de Borst, R.: Anumerical model for the cyclic densification of railway tracks. *Int. J. Numer. Meth. Engrg.*, Vol.57, No.4, pp.441-470, 2003.

[5] Koro, K., Abe, K., Ishida, M. and Suzuki, T.: Finite element simulation of the field test on the railway track with rail joints, *J. Appl. Mech. JSCE*, Vol.8, pp.1037-1047, 2005 (in Japanese).